Towards Full-Body Motion Capture of Motorcyclists In Situ–A Validation Study and User Report

Wolfgang Kremser[1], Christina Lena Groß[2], Sebastian Will[3], Raphael Pleß[3], and Tiefengrabner Martin[4]

[1]Salzburg Research, Human Motion Analytics, Salzburg, Austria
wolfgang.kremser@salzburgresearch.at (corr. author)
[2]University Salzburg, Sport and Exercise Science, Salzburg, Austria
[3]Würzburger Institut für Verkehrswissenschaften (WIVW GmbH), Veitshöchheim, Germany
[4]PIERER Innovation GmbH, Wels, Austria

Abstract

During motorcycle riding the driver's posture significantly impacts the vehicle dynamics, which makes its study important to design engineers. Current gold standard motion capture systems are unfit for in situ use due to their reliance on multiple fixed cameras. This study investigates the viability of an alternative that uses inertial sensor data called MVN Awinda. We perform concurrent validation with an optical motion capture system on a motorcycle simulator. MVN Awinda recorded some runs in excellent quality, while others had poor data quality, which calls the system's reliability into question. In runs with good data quality, MVN Awinda achieved a high correlation with the gold standard. We conclude that MVN Awinda is viable for recording general motion patterns during motorcycle driving.

1 Introduction

A motorcycle's Center of Gravity greatly influences its dynamic behavior, particularly regarding handling and stability (Cossalter, 2010). The driver's posture can shift it forwards or backward, and higher or lower, which results in either over or under steering or the slipping/lifting of a wheel (ibid.). Furthermore, depending on driving skill and style, certain groups of motorcycle drivers may react differently to various traffic and road scenarios. To build a driver-friendly and safe motorcycle, engineers may benefit from knowing the driver's actual posture in realistic conditions.

The measurement of a person's posture over time is called *motion capture*, or mocap for short. Optoelectronic mocap systems (OMS) use reflective markers and cameras and are regarded as the current gold standard (Van Der Kruk and Reijne, 2018). But they have several disadvantages when trying to measure motorcyclists *in situ*, i.e. on the road under realistic conditions. These include cost, limited observable volume, and problems working under sunlight.

An alternative to OMS is mocap based on inertial measurement units (IMUs). An IMU typically measures its three-dimensional acceleration, angular velocity, and sometimes the surrounding magnetic field. By attaching an IMU to a body segment, the segment's position and orientation can be determined by integrating the acceleration and angular velocity. This method of positioning an object in 3D space is called *strapdown inertial navigation* (Savage, 2007).

One IMU-based mocap system is Xsens MVN Awinda (Schepers *et al.*, 2018). Awinda's 17 IMUs (full-body setup) are attached to hook-and-loop straps that are fastened onto the subject's body segments at specific bone landmarks. The IMUs communicate wirelessly with a base station that is connected via USB to a PC running the software MVN Analyze. It maps the IMU data to a biomechanical model that consists of 23 body segments linked through 22 joints. The final dataset contains the segment and joint positions and orientations, as well as joint angles at a sample rate of 60Hz. Sample rates of 120Hz are available when measuring only the upper or lower body. The major advantage of MVN Awinda against OMS is its unbounded range. The base station and a small laptop can be carried along in the trunk or a backpack (Kremser *et al.*, 2024). Alternatively, one can use the MVN Link system where the IMUs are integrated into a full-body lycra suit. It

features an on-body recording unit which eliminates the need for external hardware altogether. MVN Link uses the same software package (MVN Analyze) to process the mocap data.

However, this mobility comes with reduced accuracy. IMU-based mocap systems have two major error sources. The first is soft-tissue artefacts. Since the IMUs are strapped down on top of independently moving layers like clothing, skin, and fat tissue, their position relative to a bone landmark shifts during movement. For this reason, IMU-based mocap is less accurate, especially for obese subjects (Cerfoglio *et al.*, 2023). The second error source is position and orientation drift, which are caused by the integration of noisy accelerometer and gyroscope data (Savage, 2007).

While we could not identify reports of using MVN mocap systems on motorcycles, several studies compare their accuracy against OMS in other fields. (Mavor *et al.*, 2020) recorded soldiers performing typical military activities in the field and found that the average correlation between MVN Link and their reference OMS was 0.81 ($\sigma : 0.13$). Similarly, (Al-Amri *et al.*, 2018) found excellent agreement between MVN Awinda and the OMS in the sagittal plane ($R^2 > 0.8$) and acceptable agreement ($R^2 : 0.4 - 0.8$) in the frontal and transverse planes for walking, squatting and vertical jumping. However, it is questionable whether these results translate to the dynamics of motorcycle riding, As (Robert-Lachaine *et al.*, 2017, p. 617) states: ”IMUs accuracy is affected by the complexity and duration of the tasks highlighted by increased [Root Mean Squared Error]”.

The MVN mocap systems seem promising candidates for realizing in situ mocap of motorcycle drivers, but too little is known about their behavior on moving motorcycles. Thus, the goal of this study is to characterize the error and drift of MVN Awinda on a moving motorcycle. The work presented here is an excerpt of a master thesis about mocap on moving motorcycles (Kremser, 2024).

2 Methods

2.1 Materials

2.1.1 Motorcycle Simulator & Test Driver

As suggested by the decision tree in (Will *et al.*, 2023), the validation study was performed on the DESMORI dynamic motorcycle simulator, as the cost of equipping even a short test track with the OMS would have been prohibitive. The DESMORI simulator (Figure 1) consists of a BMW F 800S as a mockup that is mounted on a hydraulic platform with six degrees of freedom. It can simulate different realistic and synthetic road layouts and traffic situations using SILAB® driving simulation software. Drivers experience simulated road and engine vibrations, and a rope-and-pulley mechanism pulls them back to simulate inertia. All driver input is recorded and can be exported for later analysis.

The test driver (age: 32, sex: male, weight: 85kg, height: 183cm) was one of the simulator’s operators and thus closely familiar with its behavior and the risks involved.

2.1.2 OMS–The Gold Standard Reference

The goal of this study is to establish *concurrent validity* with the gold standard, the OMS ’Miqus M3’ (Qualisys AB, Sweden). The Miqus series is a popular choice for the validation of biomechanical measurements (Chida *et al.*, 2024; Kanko *et al.*, 2021).

The reflective markers were positioned according to Qualisys’s predefined ’Sports’ marker set (Qualisys AB, 2021) and attached using double-sided medical tape with a thickness of 0.07mm (Figure 2). To calculate the center of the pelvis which is part of the MVN biomechanical model but not included in Qualisys’s model, two additional markers were placed on the left and right greater trochanter and the midpoint between them acted as the pelvis’s center.

Seven Miqus M3 cameras facing the simulator platform were positioned in a semi-circle with the mockup in the center. The simulator’s shiny surfaces, such as the metallic hydraulic platform and parts of the mockup, had to be covered with blankets and black tape to prevent spurious marker detection. The OMS was calibrated according to the Qualysis user manual (Qualisys AB, 2017) by moving the calibration wand through the observable volume. The coordinate system’s origin was set to be near the sacrum on the motorcycle seat by placing the L-frame from the calibration kit there.

Figure 1: Image taken during one of the recorded runs. Four of the seven Miqus M3 cameras are visible here.

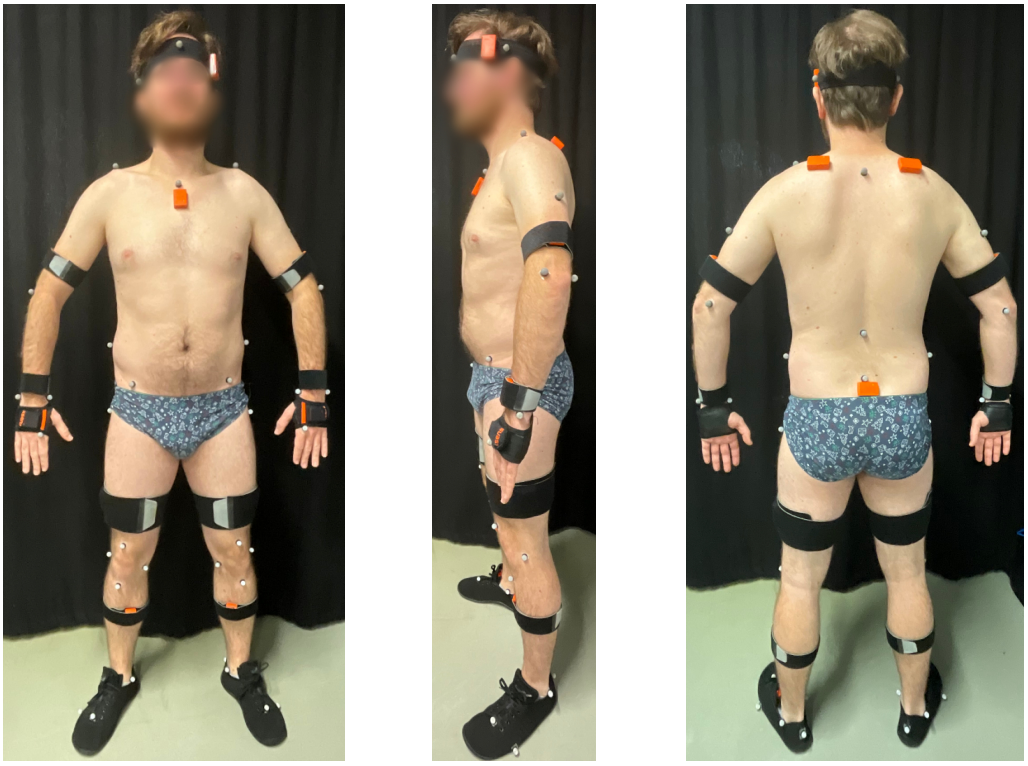

Figure 2: Front, side, and back view of the test driver with the IMUs (orange or behind the black straps) and reflective markers (gray) attached

2.1.3 MVN Awinda

After measuring the test driver's body segment lengths and entering them into MVN Analyze, he was equipped with the full-body mocap setup consisting of 17 IMUs (Figure 2) according to the MVN Awinda user manual (Movella Inc., 2023), except for the sternum and shoulder IMUs. The vest that would normally hold these IMUs would have interfered with the OMS markers, thus these IMUs were attached directly to the skin using the double-sided adhesive tape.

2.2 Data Collection

Before each recording, the MVN Awinda system was calibrated using the calibration routine programmed into MVN Analyze which involves walking a few meters. After the test driver took a seat on the simulator, the simulator operator gave the signal to ready the MVN Awinda and OMS systems. The simulation was started and a signal was given to start recording on the other two systems. After confirming that all systems were recording, the test driver was given the go to start driving. In total, more than 96 minutes of ride time were recorded over nine runs with different track layouts and driving styles (Table I).

Table I: Characteristics of the nine runs included in the analysis (CRC = constant radius cornering)

Run name	**Road layout**	**Instructions to rider**	**Duration [min]**
rural_road_01	Realistically modeled rural road with sparse traffic on both lanes	None	7.6
druecken_01	Rural road with repeating sequence of straight segments, round curves, and overtake maneuvers	”Steer by pushing”	9.0
druecken_02			8.9
hangingoff_01		”Steer by hanging off”	7.4
hangingoff_02			6.5
regular_02		”Ride as you would do normally”	8.7
regular_03			9.7
crc_01	Synthetic road layout with varying curve radii. Speed fixed via cruise control	Street signs showing how to steer (e.g. ”lean-in”, ”lean-out”)	19.8
crc_02			19.0
9 runs		**Total recorded ride time:**	**96.7**

2.3 Post-processing

Each run produced three files, one for each system. For MVN Awinda, the output files were reprocessed in HD and exported into Excel files using MVN Analyze. For the OSM, the files were exported into CSV using the QTM software. The simulator wrote its data directly into CSV files. Using custom Python scripts we converted each file into a tabular representation of a time series.

2.3.1 Aligning Biomechanical Models

One major difference between the mocap systems' biomechanical models was the 'pelvis' segment that was missing in the OMS. As mentioned above, we added two additional markers at the left and right greater trochanter and used the midpoint between these two markers as the OMS's pelvis segment. Furthermore, the body segments were labeled differently between the two mocap systems. We decided to use the labels from the MVN Awinda model and relabeled the segments from the OMS accordingly.

Initially, the coordinate systems between the two mocap systems were misaligned (Figure 3a) and thus incomparable. The handedness of the mocap systems' coordinate systems differed, with the OMS having a left-handed and MVN Awinda having a right-handed coordinate system. Furthermore, their origin was different, with the OMS's origin being at the height of the seat while MVN Awinda's origin was located at the right heel. We decided to use a left-handed coordinate system with the origin at the initial position of the pelvis and translated/rotated the data points accordingly (Figure 3b).

No further alignment of the biomechanical models was performed. However, as is visible in Figure 3b, some body segments like the head are located at significantly different places. This

is because MVN Awinda defined the origin of the 'head' segment near the neck, and the OMS defines it on the top of the head.

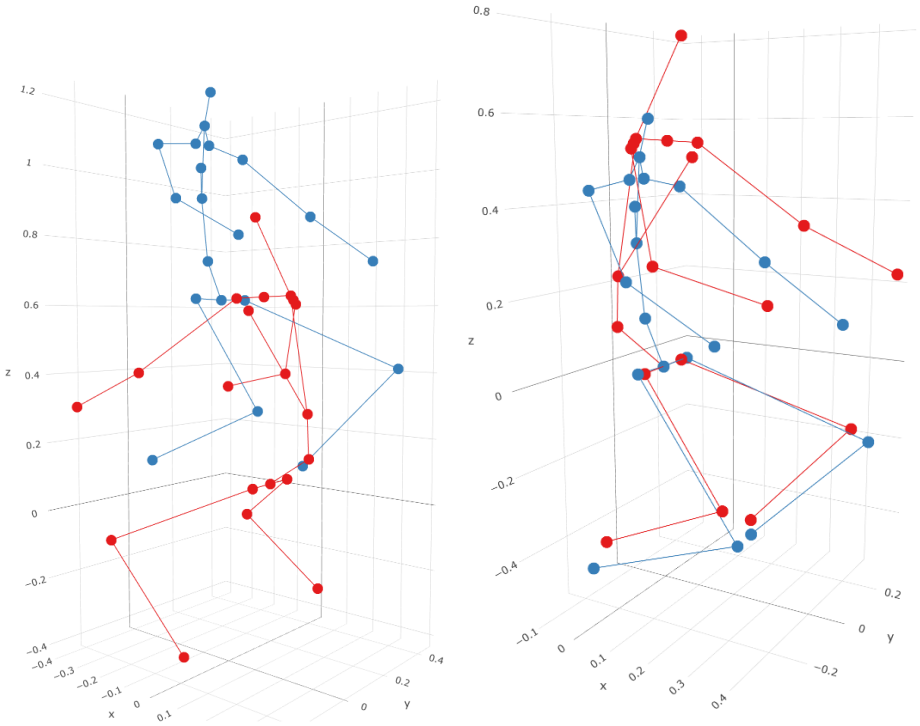

(a) Before alignment (b) After alignment

Figure 3: Isometric view of the recorded body posture at the start of a run (red = OMS, blue = MVN Awinda, axes labels in meters). (a) shows the initial miss-alignment between the systems' reference frames. But even after alignment (b), the body segments are offset due to differences in the biomechanical models' segment definitions. This is most visible with the head. The OMS defines the head's anatomical origin at the top, MVN Awinda near the base near the neck.

2.3.2 Synchronization

We used the actuation of the gear shifter to synchronize the three systems. Shifting gears produced clearly visible local minima in the downward position (z-axis) of the left foot. The time series were shifted such that the local minima first overlapped between the two mocap systems, and then with the gear data from the simulator (Figure 4). Data before the first and after the last gear shift were discarded.

2.4 Data Analysis

To compare MVN Awinda and the OMS, we use the following measures.

Consistency First, we evaluated the consistency of each mocap system. Since the lengths of body segments should remain unchanged during a run, the variance in these lengths serves as an effective measure of consistency (Venek *et al.*, 2021).

Distance between mocap systems We use the *lock-step Euclidian Distance* (LSED) (Tao *et al.*, 2021) to calculate the distance between the body segments' positions as measured by MVN Awinda and the OMS. Given two trajectories A and B, both with n samples that are identically timestamped, we define the $LSED$ as the time series

$$LSED(A,B) = (dist_2(a_1,b_1), dist_2(a_2,b_2), \ldots, dist_2(a_n,b_n)) \quad (1)$$

where $dist_2$ is the Euclidian distance between two points $a_i \in A$ and $b_i \in B$:

$$dist_2(a_i,b_i) = \sqrt{(a_i^x - b_i^x)^2 + (a_i^y - b_i^y)^2 + (a_i^z - b_i^z)^2} \quad (2)$$

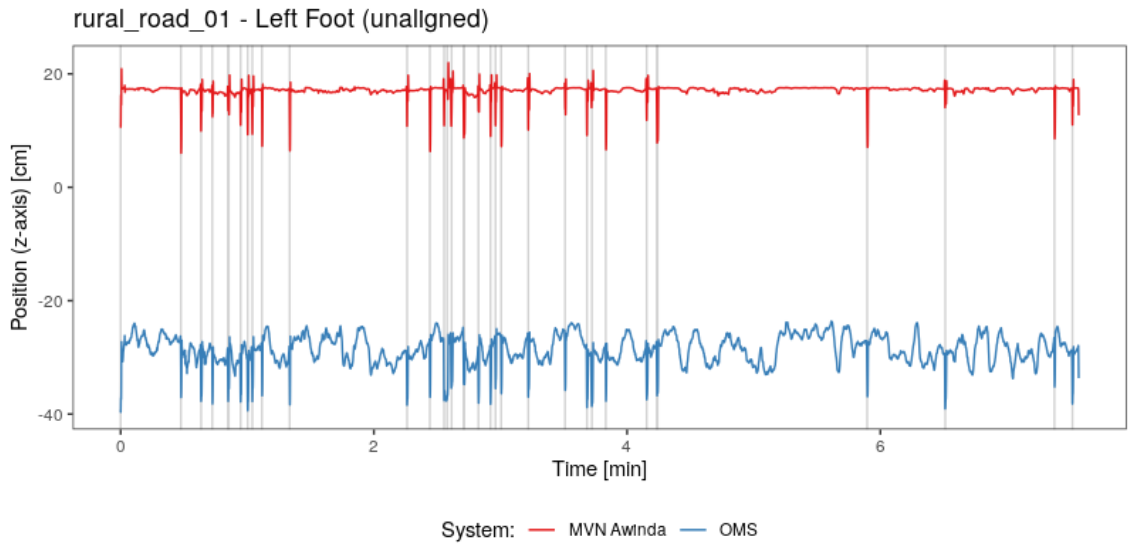

Figure 4: The motorbike's gear selector is operated with the left foot. Thus, gear switches (gray vertical lines) cause distinct local minima in the left foot's z-position. The mocap systems together with the simulator data were synchronized by overlaying these local minima with the gear switches.

The upper index refers to the points' x, y, and z components respectively.

As we have mentioned above, the body segments can be offset due to differences in the segment definition (c.f. Figure 3b). As this difference in definition cannot be considered an error, we assume that the offset is constant and subtract the $LSED$ value from the first frame from all further $LSED$ values. We call this corrected distance $LSED_0$.

Drift To identify any drift of the body segment position we fit a linear regression model of the $LSED$ over time. We do this two times: First with a biomechanical model that is free to move, and second with a model that is fixed in place at the pelvis. This way we can distinguish the drift of the whole body model from the drift of individual body segments.

Similarity As a similarity measure between MVN Awinda and the OMS we look at Pearson's correlation coefficient ρ per axis. Given two univariate time series X and Y, both of length n, it is calculated as follows (Montero and Vilar, 2014, p. 6):

$$\rho_{X,Y} = COR(X,Y) = \frac{\sum_{i=0}^{n}(X_i - \bar{X})(Y_i - \bar{Y_i})}{\sqrt{\sum_{i=0}^{n}(X_i - \bar{X})^2}\sqrt{\sum_{i=0}^{n}(Y_i - \bar{Y_i})^2}} \tag{3}$$

3 Results

3.1 Segment Length Consistency

Table II shows the median segment lengths together with their standard deviation. Ideally, no change in body segment lengths should be measured, i.e. σ should be close to zero. For the OMS, σ is between 0.0cm and 0.574cm, and for MVN Awinda the σ values are between 0.0cm and 0.570cm. Interestingly, MVN Awinda outperforms the OMS in the majority of segments, especially in the trunk section.

Table II: Mean segment lengths of the analyzed segments with their standard deviation. All values are in centimeters. Note that a body segment here is defined as the line connecting two body segment origins, therefore the "from-to" nomenclature. Lower σ values are marked with an asterisk.

Segment length		Median length		Diff.	Std. deviation	
from	to	OMS	MVN		OMS	MVN
			Upper body			
Right Upper Arm	Right Forearm	34.64	29.08	-5.56	0.000*	0.570
Right Shoulder	Right Upper Arm	8.69	13.75	5.06	0.203*	0.445
Left Upper Arm	Left Forearm	34.35	29.07	-5.28	0.000*	0.358
Left Shoulder	Left Upper Arm	8.16	13.74	5.58	0.281	0.177*
Left Forearm	Left Hand	27.13	25.37	-1.75	0.237	0.098*
Right Forearm	Right Hand	26.60	25.36	-1.23	0.147	0.009*
			Trunk			
Neck	Left Shoulder	8.16	5.90	-2.25	0.281	0.066*
Neck	Right Shoulder	8.69	5.89	-2.79	0.203	0.059*
T12	Neck	33.91	20.74	-13.17	0.31	0.009*
L5	T12	12.32	18.55	6.23	0.529	0.002*
Pelvis	L5	15.96	12.63	-3.33	0.102	0.000*
T12	T8	36.77	8.85	-27.92	0.389	0.000*
Neck	Head	25.67	9.47	-16.20	0.574	0.000*
			Lower body			
Right Foot	Right Lower Leg	40.07	45.37	5.29	0.053	0.481*
Left Foot	Left Lower Leg	40.37	45.35	4.98	0.120*	0.210
Left Upper Leg	Pelvis	8.86	10.68	1.82	0.000*	0.205
Right Upper Leg	Pelvis	8.86	10.68	1.82	0.000*	0.189
Right Lower Leg	Right Upper Leg	45.17	50.20	5.02	0.418	0.109*
Left Lower Leg	Left Upper Leg	45.94	50.19	4.25	0.434	0.008*

3.2 Similarity of Mocap Systems

The statistics for $LSED$ and $LSED_0$ are presented in Table III. The mean $LSED_0$ for most body segments falls within the millimeter range, except for the left forearm and hand, and the right lower leg and foot, where it ranges from 1.5cm to 2.85cm. The standard deviation of $LSED_0$ varies from 0.76 cm (L5) to 5.98 cm (right hand). When categorized by body region, the trunk shows the lowest $LSED_0$ ($\mu = -0.64$ cm, $\sigma = 1.1$ cm), followed by the upper body ($\mu = -0.37$ cm, $\sigma = 2.7$ cm) and the lower body ($\mu = 1.0$ cm, $\sigma = 3.08$ cm). The maximum $LSED_0$ values are relatively high, ranging from 5.9 cm (L5) to 44.58 cm (right lower leg). Out of the 22 body segments analyzed, 12 have a maximum $LSED_0$ exceeding 10 cm.

Figure 5 shows the heatmap of Pearson's correlation coefficient ρ between the OMS and MVN awinda for all three axes and all nine runes. Dark red indicates a high positive ρ value, and dark blue indicates a high negative ρ value. Light areas indicate a value close to zero, i.e. little correlation. Ideally, the mocap systems should have a high positive correlation.

The x-axis is generally lighter than the other two axes. Furthermore, the column for run 'druecken_02' is very light compared to the other columns. The column for run 'drucken_02' is the lightest among all of the runs, and it has several negative ρ values across all three axes. The columns for the runs 'crc_01', 'crc_02', and 'rural_road_01' have no negative ρ values and are mostly dark red.

Table III: Minimum, maximum, mean, and std deviation (σ) of $LSED$ and $LSED_0$ per segment

Segment	min [cm]		max [cm]		mean [cm]		σ [cm]	
	$LSED$	$LSED_0$	$LSED$	$LSED_0$	$LSED$	$LSED_0$	$LSED$	$LSED_0$
Upper body								
Left Forearm	3.63	-12.67	30.04	15.83	14.14	-1.50	4.27	3.47
Left Hand	8.42	-13.21	41.66	22.26	18.57	-1.08	6.09	4.56
Left Upper Arm	6.48	-6.94	26.68	9.67	15.62	-0.60	3.02	1.62
Left Shoulder	7.69	-3.70	19.64	8.90	12.05	-0.47	1.68	1.34
Head	16.92	-3.47	31.87	9.44	21.38	-0.40	1.72	1.23
Right Upper Arm	8.93	-7.70	29.79	14.78	15.91	-0.23	2.63	1.97
Right Forearm	3.62	-9.52	47.79	37.37	14.24	-0.10	4.21	4.91
Right Shoulder	7.01	-4.21	27.45	12.84	12.60	-0.07	1.79	1.13
Neck	3.12	-2.69	18.30	12.66	5.57	0.20	1.34	1.31
Right Hand	7.08	-8.83	48.39	31.99	18.49	0.49	5.43	5.98
Trunk								
T8	15.24	-5.60	28.72	7.87	22.45	-0.50	1.86	1.30
L5	5.70	-1.53	14.43	5.92	8.11	0.03	1.01	0.76
T12	6.04	-3.99	18.08	8.06	9.43	0.35	1.24	0.93
Neck	3.12	-2.69	18.30	12.66	5.57	0.20	1.34	1.31
Head	16.92	-3.47	31.87	9.44	21.38	-0.40	1.72	1.23
Lower body								
Left Foot	4.41	-6.36	35.53	22.92	15.00	-0.51	4.84	2.67
Left Upper Leg	1.80	-1.96	10.03	8.16	2.50	0.28	1.13	1.01
Right Upper Leg	1.70	-1.30	9.26	7.31	2.55	0.28	1.10	0.97
Left Lower Leg	4.91	-10.38	44.36	36.38	16.48	0.87	5.37	5.93
Right Lower Leg	4.41	-9.85	51.65	44.58	14.98	2.77	5.31	4.86
Right Foot	4.47	-7.96	42.36	34.40	14.17	2.84	4.29	3.05

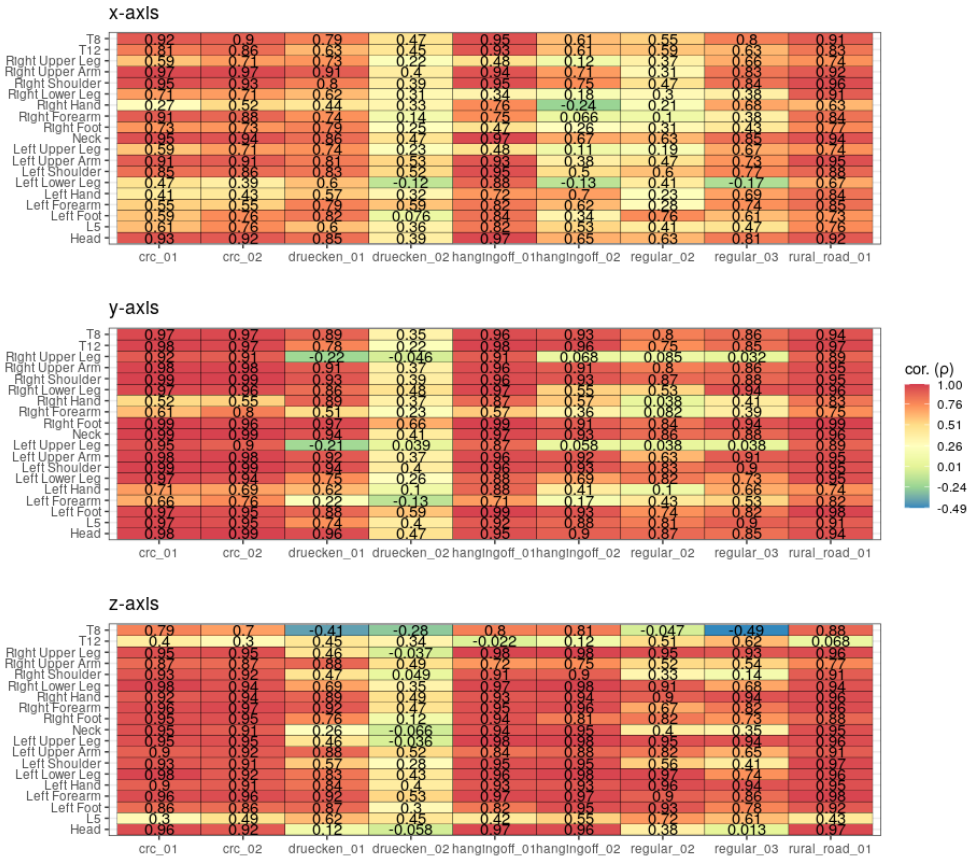

Figure 5: Heatmap of the correlation coefficients (ρ) of all segments and runs, on all three axes

3.3 Drift

Figure 6 shows the $LSED$ of the pelvis body segment plotted over time for all nine runs in the scenario where the pelvis was not fixed. In other words, this figure shows how much the entire body model drifted away from its initial position, which in turn increases the $LSED$ of the other body segments. We see some drift in all nine of the runs and on all three axes. Most dramatically on the x-axis of run `hangingoff_02`. The drift caused the body model to 'slip' off the seat and it ended up more than 60cm behind the initial position.

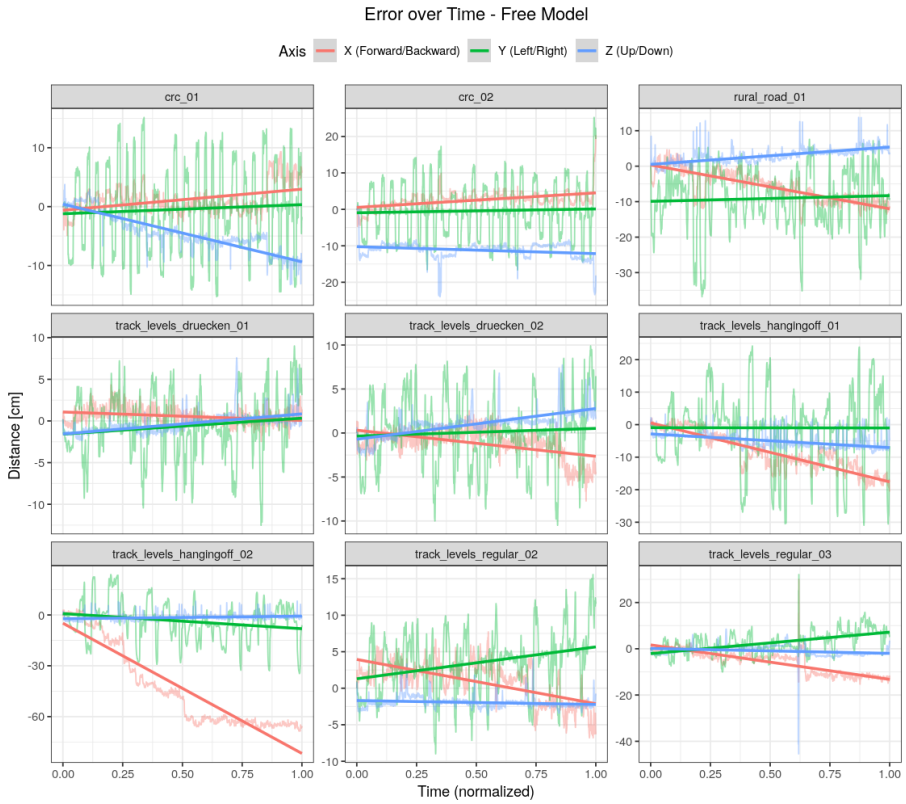

Figure 6: Time-normalized line plots of the $LSED_{Pelv}$ in pelvis position between MVN Awinda and the OMS on all three axes. The thicker lines depict the respective linear regression model $LSED_{Pelv} \sim time$.

In Table IV, we compare the drift of the extremities in the free-moving body model scenario with the scenario where the pelvis is fixed in place. While there is still a noticeable drift across the axes, it is much lower when the body model is fixed.

Table IV: Mean (μ) and standard deviation (σ) of the drift models' slopes (β)

	μ_β		σ_β	
Segment	fixed	free	fixed	free
Head	0.42	-12.29	3.07	45.22
Left Hand	-0.55	-12.02	14.69	46.32
Right Hand	0.58	-13.91	19.27	54.50
Pelvis	0.00	-13.22	0.00	44.69
Left Foot	-1.19	-15.40	7.90	45.65
Right Foot	-3.28	-13.35	9.50	45.12

4 Discussion

4.1 Reliability of MVN Awinda

We observed a large variety in data quality during our study. Figures 5 and 6 show that the drift and correlation varied widely between runs. Some runs, especially the 20-minute long `crc_01`

and `crc_02` runs were recorded in excellent quality, whereas other runs like `druecken_02` and `hangingoff_02` are practically unusable due to drift. For example, Figure 7 shows how the lower body's orientation started to drift counterclockwise and remained in this position for the rest of the run.

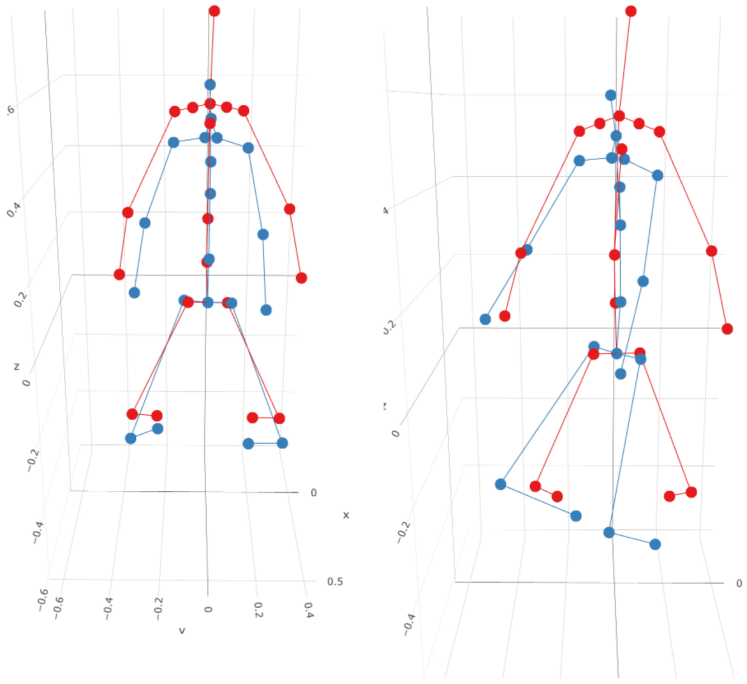

Figure 7: Frontal view of the fixed and overlayed biomechanical models (red = OMS, blue = MVN Awinda) during run 'hangingoff_02'. While the models are initially both parallel to the frontal plane (left), the MVN Awinda model starts to rotate around the longitudinal axis around the two-minute mark (right).

At the present time, we do not have an explanation for these defects in the data. We can only speculate that poor signal quality between the IMUs and base station led to data loss, or that magnetic interference from the hydraulic platform played some part.

4.2 Accuracy of MVN Awinda

In runs with good data quality, the correlation between the OMS and MVN Awinda across axes was between 0.722 and 0.831. Awinda MVN seems to have had problems with tracking the x-position ('forwards/backward') of the body segments, especially the position of the legs, the right forearm, and the right hand (ρ_x between 0.04 and 0.34). In some runs, for some body segments, the correlation even turned out negative (Figure 5).

Only 4 out of the 22 body segments had an average absolute $LSED_0$ above 1cm (left forearm and hand, right lower leg and foot) (Table III). MVN Awinda performed best in the trunk area. The lack of OMS markers on the spine might have negatively impacted the OMS's accuracy in this area, to the advantage of MVN Awinda.

The maximum $LSED_0$ values for all body segments are intolerable as they range from 5.92cm up to 51.64cm (right lower leg). Our present analysis of the $LSED_0$ distances did not distinguish by run, so we cannot say in which runs these maximum values occurred. We suspect that the high-quality runs have much lower $max(LSED_0)$ values.

Literature suggests that MVN Awinda's error increases with the dynamics of the movement, i.e. riding a curve leads to a greater error when compared to riding straight. This was not analyzed in the study. Distinguishing the runs by riding style (e.g. 'free', 'controlled', 'hanging_off', 'pushing') and analyzing its influence on $LSED_0$ would be the next step to gain a more detailed understanding of IMU-based mocap.

The conditions to compare between OMS and MVN Awinda are optimal since the subject can ride the simulator without protective gear, so the markers and IMUs are positioned directly onto the test driver's body. The simulator realistically recreates the driving dynamics of a street motorcycle

and allows for standardized traffic scenarios on both realistic and synthetic road layouts.

Researchers who want to use MVN Awinda in the future are advised to regularly check the quality of the wireless connection between IMUs and the base station, the IMUs' battery levels, and the fit of the IMUs and straps. The latter is even more important for in-situ measurements as the IMUs are probably worn under or over the protective gear. It may also be advisable to use Awinda's sibling system, the MVN Link, which integrates the IMUs into a lycra suit. This removes the Awinda base station and consequently a bad wireless connection as a potential point of failure.

5 Conclusion

This study compared the IMU-based MVN Awinda mocap system against a gold standard OMS. MVN Awinda has shown that it is capable of producing valid mocap data on a dynamic motorcycle simulator, with a high correlation to the reference OMS. The excellent performance in the two 20-minute-long runs shows that the system can work well over longer periods. However, MVN Awinda's reliability is an issue. Due to unknown circumstances, the performance seems to degrade massively after a run. Drift in position and orientation of body segments, body areas, and even the whole body make some of the collected data unusable without further postprocessing. In its current state, we can recommend MVN Awinda for in situ mocap of motorbike riders only in the 'Vehicle' scenario which holds the pelvis in place and prevents excessive drift, but this loses the information about the pelvis's movement.

References

Al-Amri, Mohammad *et al.*, (2018). "Inertial Measurement Units for Clinical Movement Analysis: Reliability and Concurrent Validity", en. *Sensors*, Vol. 18 No. 3. Number: 3, p. 719. ISSN: 1424-8220. DOI: 10.3390/s18030719. **available at**: http://www.mdpi.com/1424-8220/18/3/719 (accessed 14 Feb. 2024).

Cerfoglio, Serena *et al.*, (2023). "Assessment of an IMU-Based Experimental Set-Up for Upper Limb Motion in Obese Subjects", en. *Sensors*, Vol. 23 No. 22. Number: 22, p. 9264. ISSN: 1424-8220. DOI: 10.3390/s23229264. **available at**: https://www.mdpi.com/1424-8220/23/22/9264 (accessed 14 Feb. 2024).

Chida, Kenta *et al.*, (2024). "Assessing the validity of two-dimensional video analysis for measuring lower limb joint angles during fencing lunge", en. *Frontiers in Sports and Active Living*, Vol. 6, p. 1335272. ISSN: 2624-9367. DOI: 10.3389/fspor.2024.1335272. **available at**: https://www.frontiersin.org/articles/10.3389/fspor.2024.1335272/full (accessed 29 Feb. 2024).

Cossalter, Vittore (2010). *Motorcycle dynamics*, eng. 2. engl. ed., [Nachdr.] lulu. ISBN: 978-1-4303-0861-4.

Kanko, Robert M. *et al.*, (2021). "Concurrent assessment of gait kinematics using marker-based and markerless motion capture", en. *Journal of Biomechanics*, Vol. 127, p. 110665. ISSN: 00219290. DOI: 10.1016/j.jbiomech.2021.110665. **available at**: https://linkinghub.elsevier.com/retrieve/pii/S0021929021004346 (accessed 29 Feb. 2024).

Kremser, Wolfgang (2024). *Evaluation of an Inertial Full-Body Motion Capture System for Tracking the Pose of Motorbike Riders In Situ*, MA thesis. Paris-Lodron University Salzburg. **available at**: https://eplus.uni-salzburg.at/Abschlussarbeiten/content/titleinfo/10351924.

Kremser, Wolfgang *et al.*, (2024). "Towards Validated Head Tracking On Moving Two-Wheelers", *Data Science—Analytics and Applications*. Ed. by Haber, Peter, Lampoltshammer, Thomas J., and Mayr, Manfred. Springer Nature Switzerland: Cham, pp. 91–93. ISBN: 978-3-031-42170-9 978-3-031-42171-6. DOI: 10.1007/978-3-031-42171-6_13. **available at**: https://link.springer.com/10.1007/978-3-031-42171-6_13 (accessed 6 Nov. 2024).

Mavor, Matthew P. *et al.*, (2020). "Validation of an IMU Suit for Military-Based Tasks", en. *Sensors*, Vol. 20 No. 15, p. 4280. ISSN: 1424-8220. DOI: 10.3390/s20154280. **available at**: https://www.mdpi.com/1424-8220/20/15/4280 (accessed 20 Feb. 2024).

Montero, Pablo and Vilar, José A. (2014). "TSclust: An R Package for Time Series Clustering", en. *Journal of Statistical Software*, Vol. 62 No. 1. ISSN: 1548-7660. DOI: 10.18637/jss.v062.i01. **available at**: http://www.jstatsoft.org/v62/i01/ (accessed 6 Mar. 2024).

Movella Inc. (2023). *Awinda User Manual*, **available at**: https://wsdocs.movella.com/dot-pro-/-mtw-awinda (accessed 29 Feb. 2024).

Qualisys AB (2017). *How to Calibrate*, **available at**: https://cdn-content.qualisys.com/2018/02/8-How-to-calibrate.pdf (accessed 29 Feb. 2024).

— (2021). *How to apply the Qualisys sports marker set*, en. **available at**: https://www.qualisys.com/my/qacademy/ (accessed 8 Mar. 2024).

Robert-Lachaine, Xavier *et al.*, (2017). "Validation of inertial measurement units with an optoelectronic system for whole-body motion analysis", en. *Medical & Biological Engineering & Computing*, Vol. 55 No. 4, pp. 609–619. ISSN: 0140-0118, 1741-0444. DOI: 10.1007/s11517-016-1537-2. **available at**: http://link.springer.com/10.1007/s11517-016-1537-2 (accessed 20 Feb. 2024).

Savage, Paul G. (2007). *Strapdown analytics*, eng. 2. ed. Strapdown Associates. ISBN: 978-0-9717786-0-3.

Schepers, Martin, Giuberti, Matteo, and Bellusci, Giovanni (2018). "Xsens MVN: Consistent Tracking of Human Motion Using Inertial Sensing", en. Publisher: Unpublished. DOI: 10.13140/RG.2.2.22099.07205. **available at**: http://rgdoi.net/10.13140/RG.2.2.22099.07205 (accessed 14 Feb. 2024).

Tao, Yaguang *et al.*, (2021). "A comparative analysis of trajectory similarity measures", en. *GIScience & Remote Sensing*, Vol. 58 No. 5, pp. 643–669. ISSN: 1548-1603, 1943-7226. DOI: 10.1080/15481603.2021.1908927. **available at**: https://www.tandfonline.com/doi/full/10.1080/15481603.2021.1908927 (accessed 25 Mar. 2024).

Van Der Kruk, Eline and Reijne, Marco M. (2018). "Accuracy of human motion capture systems for sport applications; state-of-the-art review", en. *European Journal of Sport Science*, Vol. 18 No. 6. Number: 6, pp. 806–819. ISSN: 1746-1391, 1536-7290. DOI: 10.1080/17461391.2018.1463397. **available at**: https://www.tandfonline.com/doi/full/10.1080/17461391.2018.1463397 (accessed 29 Nov. 2023).

Venek, Verena, Kremser, Wolfgang, and Stöggl, Thomas (2021). "Towards a Live Feedback Training System: Interchangeability of Orbbec Persee and Microsoft Kinect for Exercise Monitoring", en. *Designs*, Vol. 5 No. 2, p. 30. ISSN: 2411-9660. DOI: 10.3390/designs5020030. **available at**: https://www.mdpi.com/2411-9660/5/2/30 (accessed 14 Mar. 2024).

Will, Sebastian *et al.*, (2023). "Simulator validation – a new methodological approach applied to motorcycle riding simulators", en. *The Evolving Scholar - BMD 2023, 5th Edition*. The Evolving Scholar - BMD 2023, 5th Edition. DOI: 10.59490/65046ee9de99f2072e9d1734. **available at**: https://dapp.orvium.io/deposits/65046ee9de99f2072e9d1734/view (accessed 21 Nov. 2023).